

Synthesis of Nanocomposite Based on α -Fe₂O₃ Supported on Oxidized Graphene and Its Electrochemical Characteristics

Hadeel M. Banbela^{1,2}, Laila M. Alharbi¹, Mohamed Abdel Salam^{1,*}

¹ Department of Chemistry, Faculty of Science, King Abdulaziz University, P.O Box 80200-Jeddah 21589, Saudi Arabia

² Chemistry Department, College of Science and Arts at Khulis, University of Jeddah, P.O. Box 80327, Jeddah 21589, Saudi Arabia

*E-mail: mabdelsalam@kau.edu.sa

Received: 2 February 2022 / Accepted: 12 March 2022 / Published: 5 April 2022

In this research work, hematite (α -Fe₂O₃) nanoparticle, and oxidized graphene (OG) were prepared, and then mixed to form stable suspension of α -Fe₂O₃/OG nanocomposite. Different characterization techniques were used to explore the chemical and physical properties of the α -Fe₂O₃/OG nanocomposite including XRD, FT-IR, and UV-Vis. The results revealed the successful formation of the α -Fe₂O₃ nanoparticles, and the oxidation of the MWCNT, as well as the formation of stable α -Fe₂O₃/OG nanocomposite. The electrochemical behaviour of the α -Fe₂O₃/OG nanocomposite were investigated using cyclic voltammetric (CV), and linear sweep voltammetry (LSV) and the results revealed that modification of α -Fe₂O₃ nanoparticles with OG greatly enhanced the electrochemical performance, and capacitive behaviour, as well as the cycling stability.

Keywords: hematite nanoparticle; oxidized graphene, capacitive behaviour; electrochemical behaviour

1. INTRODUCTION

Nanotechnology is a general term focused on the manipulation and applications of nanoparticles (NPs) such as metals, metal oxides, semiconductors, ceramics, and polymers, due to their outstanding structural, physicochemical and morphological properties, which allows them to be the used in a wide variety of applications, especially in the energy sector. For example, many metal oxides were used recently as electrodes for the lithium-ion batteries (LIBs) due to their outstanding and efficient surface area, as well as the chemical suitability and stability, as they intercalate–deintercalate lithium ions into their layered structure [1-3], which significantly enhanced the LIBs storage capacities even beyond their theoretical values [4]. Hematite (α -Fe₂O₃) nanostructures is one of the promising metal oxide

nanoparticles which attracted the attention of researchers, and is used for a variety of applications including splitting of water and the production of hydrogen gas [5], magnetic storage devices [6], potential gas sensors [7], targeted drug delivery [8], biomedical applications [9], as well as LIBs production [10–13].

Oxygen evolution reaction (OER) have become the common power source for sustainable energy development technology especially the photoelectrochemical (PEC) cells. The electro-catalysts of non-noble metal has been very interesting in this field, reportedly hematite has an outstanding performance of oxygen evolution reaction (OER), with an optical narrow bandgap around ~ 2.2 eV, which it absorbs the light up to 560 nm, which allows it to absorb 40% of the solar irradiance. Hematite is a naturally abundant, low-cost material that has good chemical stability in an aqueous solution in a broad pH range. The position of the valence band is suitable for oxygen evolution, which makes it an ideal candidate photoanode material for solar water splitting [14,15]. On the other hand, hematite has shown low efficiency because of its poor electrical conductivity. The critical reasons are high recombination of electrons and holes, low mobility of the holes/short hole diffusion length and trapping of electrons by oxygen deficiency sites. Various techniques are reported in the literature to improve the efficiency of hematite by inserting the effective materials in the lattice without disturbing the structure of crystal. Enhancing the efficiency of hematite for photoelectrochemical water splitting was carried out by doping with elements/ions such as tin [16], manganese [17], zirconium and tin [18], tantalum [19], boron [20], phosphorous [21], rhodium [22], tetravalent dopants (Si^{4+} , Sn^{4+} , Ti^{4+} , and Zr^{4+}) [23], and few works were dedicated to doping with carbon based materials such as carbon dots [24, 25], graphene [26,27], and the number of studies focusing on this topic is very scarce in literature.

In this work, the electrochemical behaviour of the hematite/oxidized graphene (OG) nanocomposite was studied and explored. First, hematite was prepared using hydrothermal method, and then mixed with the OG to form a stable nanocomposite. The hematite/OG nanocomposite was then characterized by XRD in order to explore the chemical and physical characteristics. The electrochemical behaviour of the hematite/OG nanocomposite was investigated using cyclic voltammetric (CV) and linear sweep voltammetry (LSV) to explore their possible applications.

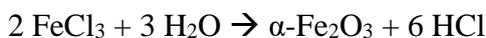
2. EXPERIMENTAL

2.1 Chemicals and materials

Ferric chloride hexahydrate ($\text{FeCl}_3 \cdot 6\text{H}_2\text{O}$) was obtained from Lobachemie and were used as received without further purification. Graphene nanosheets were obtained from XG Science (xGnP® 300, USA) and were used as received. Sulfuric acid - 95-99% (H_2SO_4) and nitric acid - 65% (HNO_3) were purchased from Chem-Lab. Potassium hydroxide (KOH) was obtained from Fluka Chemie AG. All aqueous solutions were prepared with distilled water.

2.2. Preparation of Hematite (α -Fe₂O₃) Nanoparticles

The Hematite nanoparticles were prepared according to the procedure used by Faust et al.[28]. Initially, 30 ml solution of 0.1 M FeCl₃ · 6 H₂O was dissolved in distilled water and added dropwise into 120 ml stirred boiling water, and subsequently the solution was refluxed for 5 min. Finally, cooled in an ice bath. The colloidal α -Fe₂O₃ suspension had a dark red color and was very acidic:



The colloid was dialyzed by using a dialysis tube (Medicell International, MWCO 12000 - 14000) in the distilled water, which change several times until the pH had reached pH ~ 6 and the electrical conductivity was below 20 S cm⁻¹. The product was kept in the dark.

2.3. Oxidation of graphene

The raw graphene are not reactive. In this work, the purification and activation of Graphene were in the presence of oxidation agents: H₂SO₄/HNO₃ mixture to formation of functional groups: hydroxyl, carboxyl, aldehyde, anhydride and other groups on the defected sides of the tubes, which makes them more reactive.

The acid mixtures were prepared in an ice bath. Firstly, 1 g of Graphene was used with the acid mixtures H₂SO₄/HNO₃ at the ratio of 3:1 (v/v) in a total volume of 200 ml of acid mixtures in an ice bath. The reactions were sonicated for 4 hours in an ultrasonic bath at 40°C. The resulting solution was then transferred to a 1000 ml beaker with distilled water to reduce the acidity of product, which was then neutralized by using a dialysis tube (Medicell International, MWCO 12000 - 14000) in the distilled water, that were changed several times until achieving a neutral pH.

2.4. Preparation of α -Fe₂O₃/OG nanocomposite

The hematite was deposited on the surface of oxidized graphene by mixing at RT for one hour under ultrasonication with different concentrations of graphene. All prepared suspensions before and after mixing were dried overnight in oven at 50°C. For further characterization, then the solutions and the powder were obtained in the dark. For XRD measurements, the resulting powder was calcined at 200°C for 2 h at a heating rate of 5°C · min⁻¹ in a preheated muffle furnace.

2.5. Electrode fabrication

α -Fe₂O₃ and α -Fe₂O₃/OG electrodes have been prepared for electrochemical investigations. Approximately 50 μ l of the prepared suspensions has been directly drop-cast [29] onto the glassy carbon electrode (GCE) in a rotating ring disk electrode system (RRDE), which has been used as a working electrode.

2.6. Characterization

The optical absorptions of the prepared hematite with different pH-values were investigated by using a MultiSpec-1501 UV-Vis Spectrophotometer (SHIMADZU). The determination of functional group on the surface of Graphene was performed with a PerkinElmer Spectrum 100 infrared spectrometer (FT-IR spectra), wherefore the dried samples was mixed with potassium bromide (ratio of 1:10) and pressurized to produce KBr pellet for FT-IR measurements. The identification of crystalline phases of the samples were recorded by Bruker D2 Phaser X-ray diffractometer. The XRD-measurements were carried out by $\text{CuK}\alpha$ radiation (1.5418 Å).

2.7. Electrochemical measurements

The electrochemical measurements include cyclic voltammetric (CV) studies, and linear sweep voltammetry (LSV) studies were performed using CorrTest electrochemical workstation with a RRDE three-electrode system. The working electrodes were fabricated by drop-casting a sample as described in the experimental section (2.5). The Ag/AgCl was the reference electrode and Pt wire the counter electrode in 1.0 M KOH as electrolyte. CV and LSV curves of $\alpha\text{-Fe}_2\text{O}_3$ were recorded at potential of 100 Hz and with scan rate of 100 mV s^{-1} .

3. RESULTS AND DISCUSSION

3.1. Characterization

Fig. 1 shows the optical properties of $\text{FeCl}_3 \cdot 6 \text{H}_2\text{O}$ and the freshly prepared hematite nanoparticles with pH-value ~ 6 by using UV-Vis absorption spectroscopy.

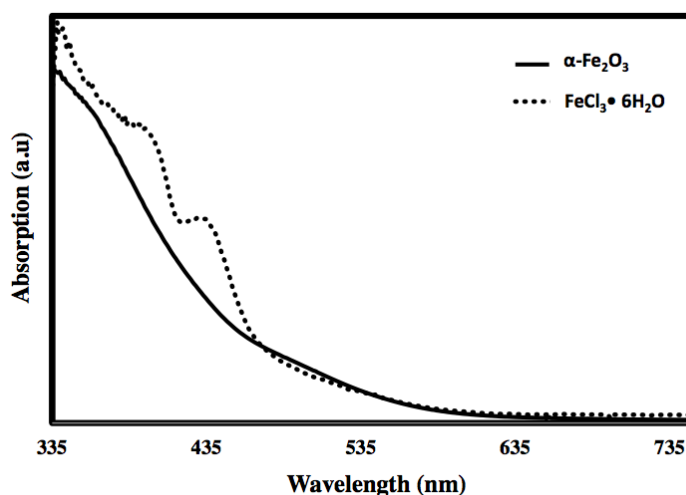


Figure 1. The UV-Visible absorption curves of hematite nanoparticles.

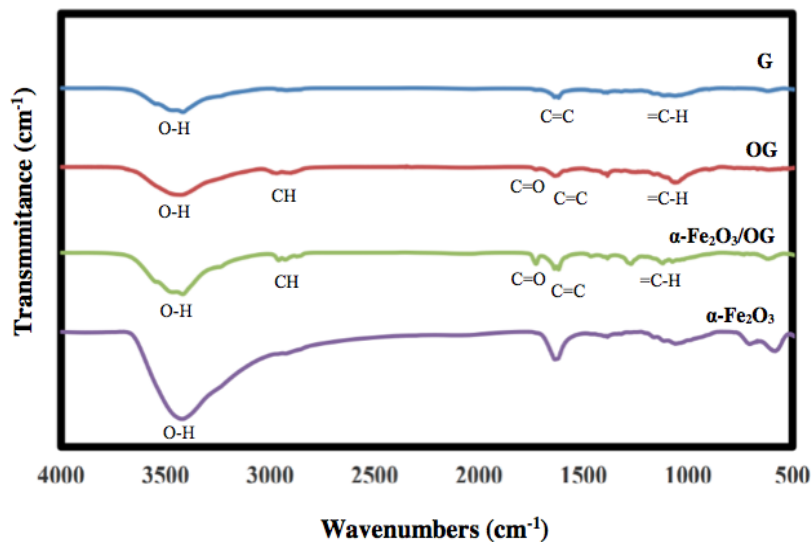


Figure 2. FT-IR spectra of graphene, oxidized graphene, hematite nanoparticles, and hematite/OG nanocomposite.

The absorption of the colloidal $\alpha\text{-Fe}_2\text{O}_3$ begins below 560 nm, which indicates that prepared $\alpha\text{-Fe}_2\text{O}_3$ is a visible light active photocatalyst. According to Sivula [5] the absorption below 560 nm is due to the absorption of shorter wavelengths of visible region (yellow to ultraviolet photons). Thus, as a result of good transmission of red light, this becomes the characteristic red color of hematite.

FT-IR was used to investigate the successful oxidation of the OG and preparation of the $\alpha\text{-Fe}_2\text{O}_3$, as well as the $\alpha\text{-Fe}_2\text{O}_3/\text{OG}$ nanocomposite, and the results were shown in Figure 2. The FT-IR spectrum of the pristine G showed the characteristic vibration peaks at 1680-1640 cm^{-1} (C=C stretch) and 1500-1400 cm^{-1} (C-C stretch) due to the carbon hexagonal ring of the graphene. In contrast, the oxidized graphene (OG) spectrum show very clear and strong absorption peak at 1730 cm^{-1} , and weak peak at 1130 cm^{-1} , which could be attributed to the stretching vibration of C=O corresponding to the stretching vibration of C=O from the carboxylic acid groups (-COOH), and C-O stretch from either a phenol or lactone; which confirmed the successful oxidation of the G [30]. The FT-IR spectrum of $\alpha\text{-Fe}_2\text{O}_3$ showed the characteristic Fe-O sharp peaks at 478 cm^{-1} and 568 cm^{-1} due to the vibrational mode [31]. Furthermore, the FT-IR spectrum of $\alpha\text{-Fe}_2\text{O}_3/\text{OG}$ nanocomposite showed three new peaks at the range of 1760- 1100 cm^{-1} appears after the mixing of the $\alpha\text{-Fe}_2\text{O}_3$ with OG, and band shifting occurs from 600 to 628 cm^{-1} , which indicated that the hematite surface was modified by the oxidized G. A broad peak at approximately 3500 cm^{-1} for all the investigated samples, which could be assigned to O-H stretch, due to moisture, alcohol or phenol, OH⁻ or carboxylic groups in these samples.

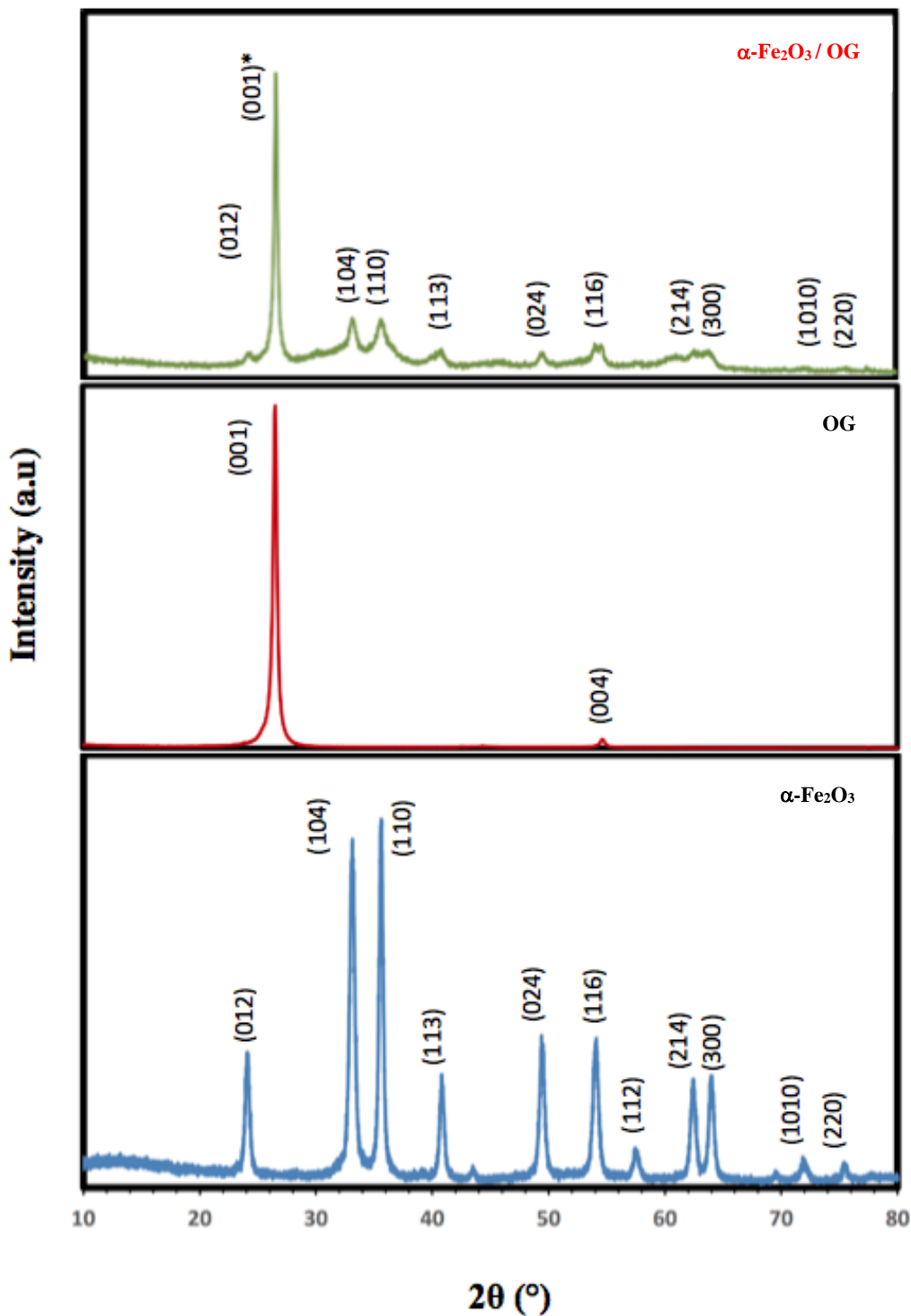


Figure 3. XRD of hematite nanoparticles, oxidized G, and hematite/OG nanocomposite.

Figure 3 illustrates the XRD patterns of the prepared $\alpha\text{-Fe}_2\text{O}_3$ nanoparticles, OG and the $\alpha\text{-Fe}_2\text{O}_3/\text{OG}$ nanocomposite. According to the XRD, the characteristic peaks of hexagonal crystal system $\alpha\text{-Fe}_2\text{O}_3$ nanoparticles were identified from the diffraction peaks at $2\theta = 24.20^\circ, 33.21^\circ, 35.70^\circ, 40.92^\circ, 49.60^\circ, 54.15^\circ, 57.90^\circ, 62.50^\circ,$ and 64.10° related to the (012), (104), (110), (113), (024), (116), (112), (214), and (300), respectively (JCPDS card no 96-900-9783). Moreover, the sharp peaks of the $\alpha\text{-Fe}_2\text{O}_3$

nanoparticles indicates the highly crystalline structure of the hexagonal crystal system, with average crystallite size of 18.55 nm as calculated from the Scherer equation. On the other hand, OG exhibit two diffraction peaks; one at 26.14° (002 plane) and the other 20.00° (100 plane), corresponding to graphitic carbon (JCPDS card #8-415). Furthermore, the XRD pattern of the α -Fe₂O₃/OG nanocomposite exhibits the characteristic peaks of both hexagonal crystal system of α -Fe₂O₃ nanoparticles and the oxidized G.

3.2. Electrochemical measurements

The prepared α -Fe₂O₃ nanoparticles and its nanocomposite was investigated as electrode material for supercapacitors, and the electrochemical properties were investigated using cyclic voltammetry (CV), and linear sweep voltammetry (LSV). Figure 4 shows the cyclic voltammograms of the prepared α -Fe₂O₃, OG, and α -Fe₂O₃/OG nanocomposite in a 1.0 mol/L KOH solution in the potential window range -0.3 V of to 0.6 V. In general, the CV of the prepared α -Fe₂O₃ nanoparticles exhibited rectangular-shaped and without redox peaks, indicating the pseudocapacitive behavior with fast and reversible surface reactions indicating good capacitive characteristics and suggest that the α -Fe₂O₃ nanoparticles electrode is an excellent candidate for electrochemical double-layer capacitors, and the consistent CV indicated that the prepared α -Fe₂O₃ nanoparticles exhibited regular capacitive behaviour and excellent cycling stability [32,33].

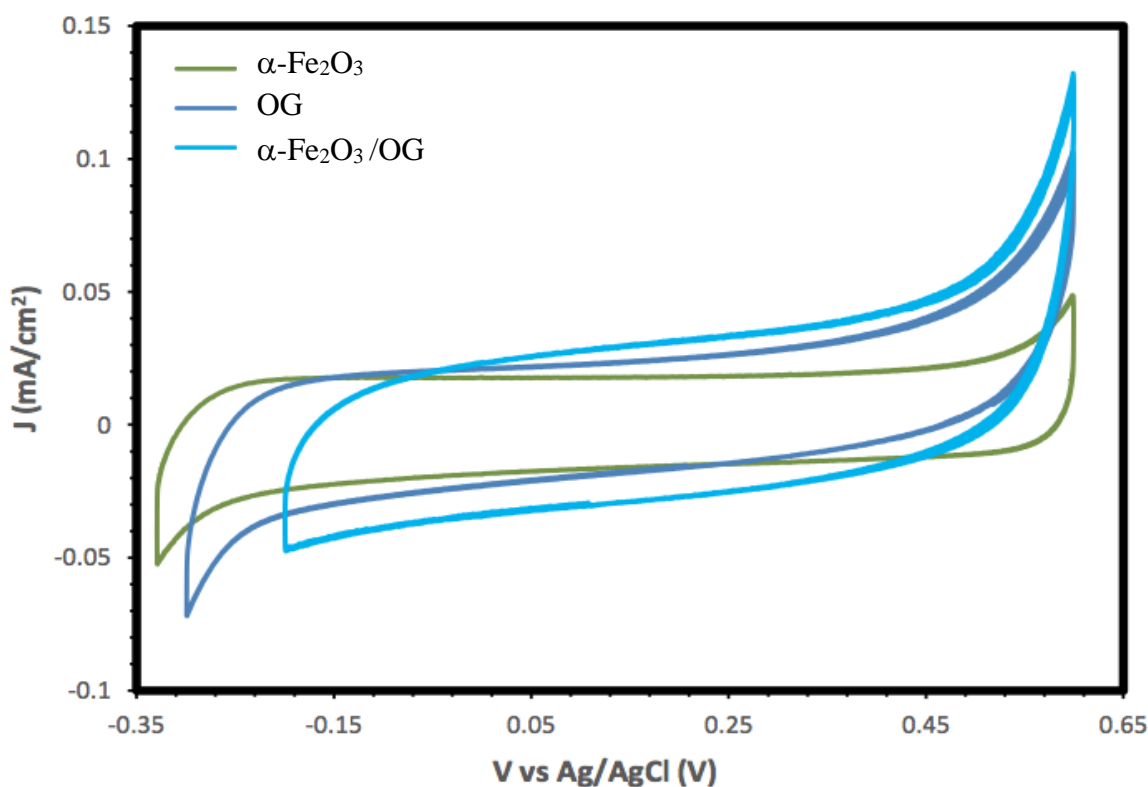


Figure 4. Cyclic voltammetry of OG, α -Fe₂O₃ nanoparticles and α -Fe₂O₃/OG nanocomposites in 1.0 M KOH.

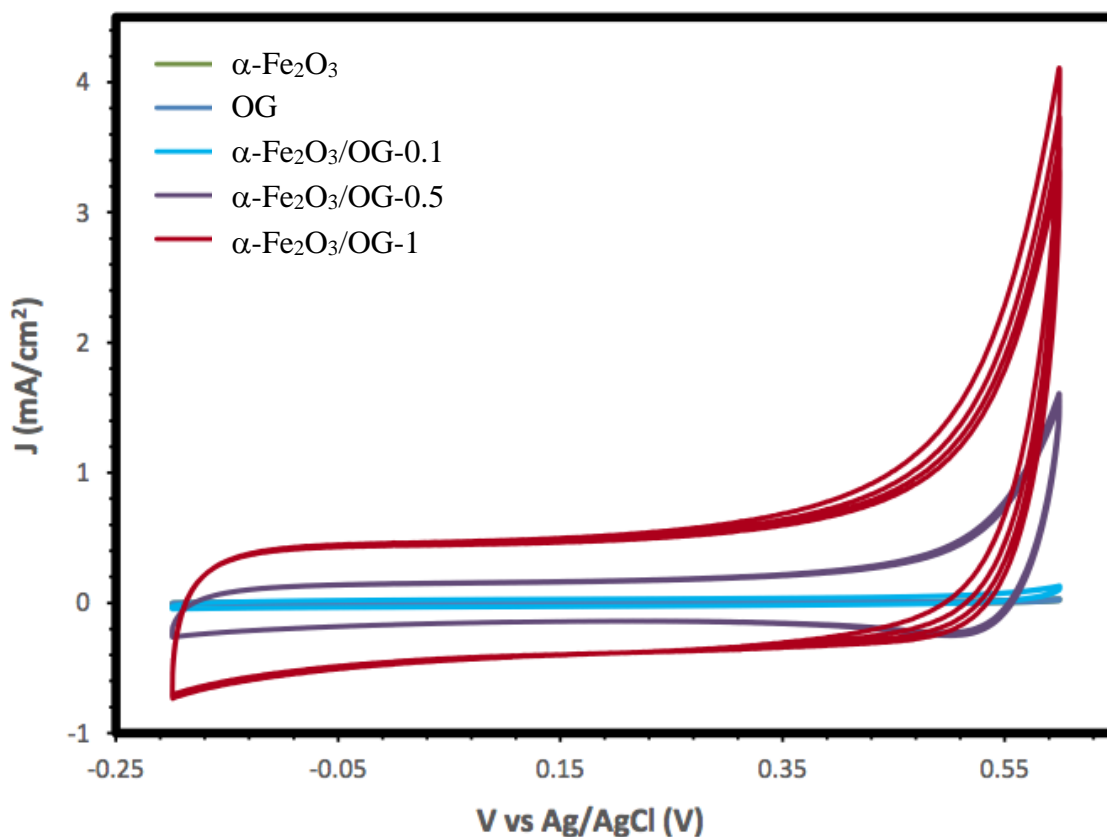


Figure 5. The variation of the cyclic voltammetry of $\alpha\text{-Fe}_2\text{O}_3$ /OG nanocomposites with different amount OG. [$\alpha\text{-Fe}_2\text{O}_3$ /OG-0.1 (0.1 ml OG was used), $\alpha\text{-Fe}_2\text{O}_3$ /OG-0.5 (0.5 ml OG was used), and $\alpha\text{-Fe}_2\text{O}_3$ /OG-1 (1.0 ml OG was used)]

The voltammogram of the OG showed a typical double layer behavior, and the featureless CV probably results from the variations in length, diameter, and helicity of the arrangement of carbon hexagon rings at the working electrode [34]. On the other hand, the voltammogram of the $\alpha\text{-Fe}_2\text{O}_3$ /OG nanocomposite showed the same characteristics of the pseudocapacitive behavior similar to the $\alpha\text{-Fe}_2\text{O}_3$, but with higher current density compared with both $\alpha\text{-Fe}_2\text{O}_3$, and OG; especially the cathodic current, which may indicate the enhancement of the reductive dissolution of the $\alpha\text{-Fe}_2\text{O}_3$ surface in the presence of the OG, and the total capacitance is a result of $\alpha\text{-Fe}_2\text{O}_3$ pseudo-capacitance and EDLC capacitance of the OG. Moreover, the variation of the OG within the $\alpha\text{-Fe}_2\text{O}_3$ /OG nanocomposite had a significant effect as it is presented in Figure 5, as the current density was increased with increasing the amount of OG within the $\alpha\text{-Fe}_2\text{O}_3$ /OG nanocomposite, which may be attributed to the enhancement of the specific surface area of the $\alpha\text{-Fe}_2\text{O}_3$ electrode upon the mixing with more oxidized graphene.

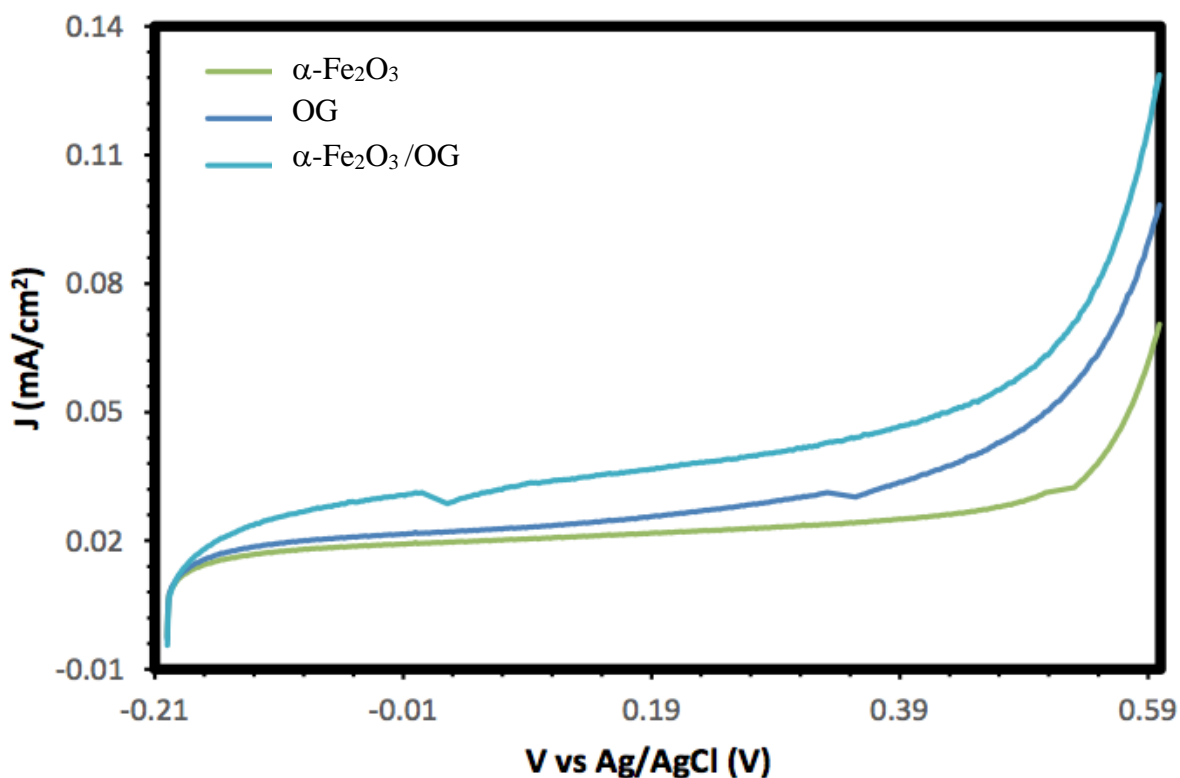


Figure 6. Linear sweep voltammograms (LSV) of OG, α -Fe₂O₃ nanoparticles and α -Fe₂O₃/OG nanocomposites in 1.0 M KOH.

Figure 6 showed the Linear sweep voltammograms (LSV) of OG, α -Fe₂O₃ nanoparticles, and α -Fe₂O₃/OG nanocomposite (1.0 ml OG) in 1.0 M KOH. It is clear from the figure that the generated current of the α -Fe₂O₃ nanoparticles greatly enhanced upon the addition of the OG indicating the performance improvement for the photoelectrochemical (PEC) application [35-40], which enhanced greatly in the presence of more OG; as it is presented in Figure 7. This enhancement in the PEC performance could be due to the change in the morphology, and the hydrophilicity of the interface and consequently the faradic current upon the addition of the OG, which may presented in Figure 8, as the charging current enhancement is greatly dependant on the amount of OG loaded.

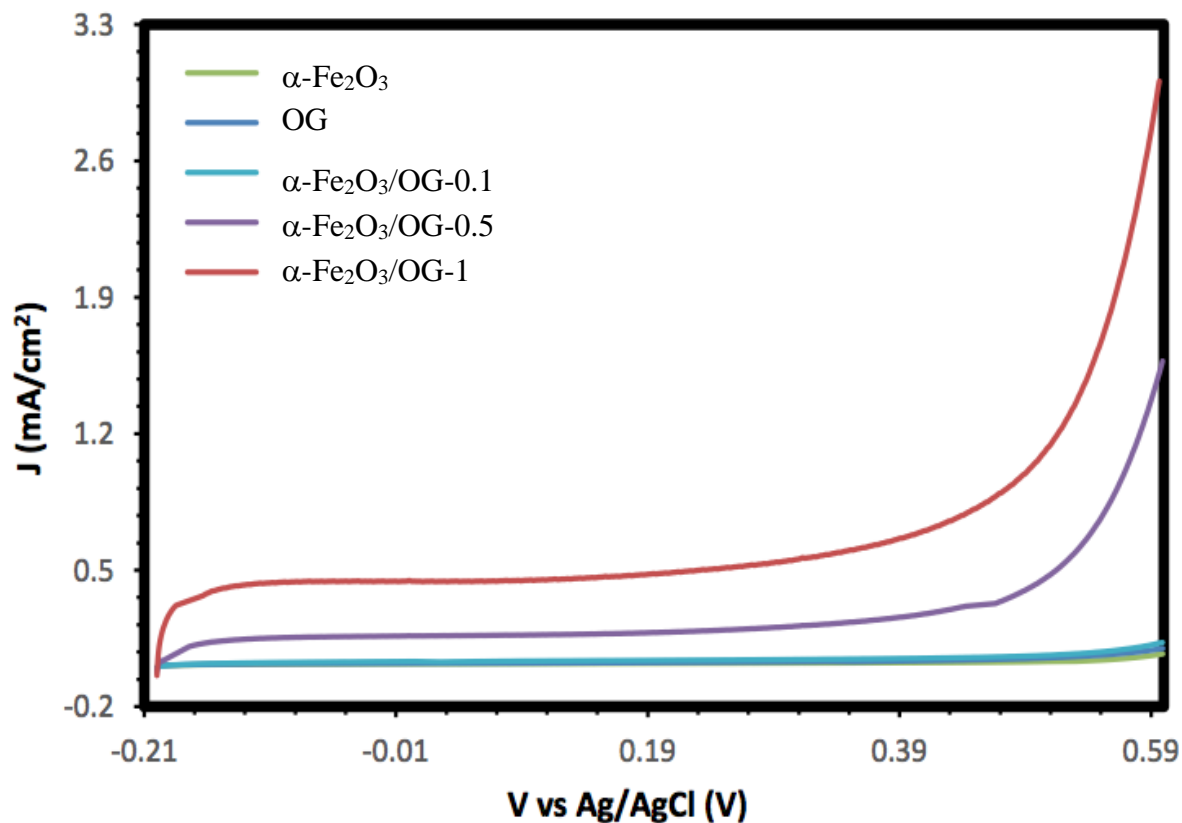


Figure 7. The variation of the current density with the potential for $\alpha\text{-Fe}_2\text{O}_3/\text{OG}$ nanocomposites with the amount OG. [$\alpha\text{-Fe}_2\text{O}_3/\text{OG}-0.1$ (0.1 ml OG was used), $\alpha\text{-Fe}_2\text{O}_3/\text{OG}-0.5$ (0.5 ml OG was used), and $\alpha\text{-Fe}_2\text{O}_3/\text{OG}-1$ (1.0 ml OG was used)]

4. CONCLUSIONS

$\alpha\text{-Fe}_2\text{O}_3/\text{OG}$ nanocomposite was successfully prepared using wet chemistry, and then were characterized chemically and physically using different characterization techniques. UV-Vis absorption spectroscopy showed the absorption of the colloidal $\alpha\text{-Fe}_2\text{O}_3$ begins below 560 nm, indicating that the prepared $\alpha\text{-Fe}_2\text{O}_3$ is a visible light active photocatalyst, and the FT-IR measurements showed the successful oxidation of the graphene and preparation of the $\alpha\text{-Fe}_2\text{O}_3$, as well as the $\alpha\text{-Fe}_2\text{O}_3/\text{OG}$ nanocomposite, through the presence of their characteristic vibration peaks, whereas the XRD measurements showed the characteristic diffraction peaks of graphitic carbon nanotubes. The electrochemical behaviour of the $\alpha\text{-Fe}_2\text{O}_3/\text{OG}$ nanocomposite was investigated using cyclic voltammetric (CV), and linear sweep voltammetry (LSV), and the results revealed that modification of $\alpha\text{-Fe}_2\text{O}_3$ nanoparticles with OG greatly enhanced the electrochemical performance, and capacitive behaviour, as well as the cycling stability.

References

1. G. Nazri, G. Pistoia, Lithium Batteries: Science and Technology. Kluwer Academic, New York 2003.

2. P. Poizot, S. Laruelle, S. Grugeon, L. Dupont, J. Tarascon. *Nature*, 407 (2000) 496.
3. A. S. Arico, P. G. Bruce, B. Scrosati, J. Tarascon, W. V. Schalkwijk, *Nat. Mater.*, 4 (2005) 366.
4. Q. Li, H. Li, Q. Xia, Z. Hu, Y. Zhu, S. Yan, C. Ge, Q. Zhang, X. Wang, X. Shang, S. Fan, Y. Long, L. Gu, G. Miao, G. Yu, J. S. Moodera, *Nat. Mater.*, 20 (2021) 76.
5. K. Sivula, F. L. Formal, M. Grätzel, *ChemSusChem*, 4 (2011) 432.
6. B. Sharma, A. Sharma, *Appl. Surf. Sci.*, 567 (2021) 150724.
7. N. V. Long, T. Teranishi, Y. Yang, C. M. Thi, Y. Cao, M. Nogami, *Inter. J. Metall. Mater. Eng.*, 1 (2015) 1.
8. T. Vangijzegem, D. Stanicki, S. Laurent, *Expert Opin. Drug Deliv.*, 16 (2019) 69.
9. J. Singh, M. Srivastava, J. Dutta, P. K. Dutta, *Int. J. Biol. Macromol.*, 48 (2011) 170.
10. C. Wu, P. Yin, X. Zhu, C. OuYang, Y. Xie, *J. Phys. Chem. B*, 2006, 110, 36, 17806–17812.
11. L. Xu, Y. Tian, T. Liu, H. Li, J. Qiu, S. Li, H. Li, S. Yuan, S. Zhang, *Green Energy Environ.*, 3 (2018) 156.
12. Y. Lin, P. R. Abel, A. Heller, C. B. Mullins, *J. Phys. Chem. Lett.*, 2 (2011) 2885.
13. J. Yao, Y. Yang, Y. Li, J. Jiang, S. Xiao, J. Yang, *J. Alloys Compd.*, 855 (2021) 157288.
14. M. Muhajir, P. Puspitasari, J. A. Razak, *J. Mech. Sci. Technol.*, 3 (2020) 51.
15. B. Iandolo, B. Wickman, I. Zorić, A. Hellman, *J. Mater. Chem. A*, 3 (2015) 16896.
16. Y. Ling, G. Wang, D. A. Wheeler, J. Z. Zhang, Y. Li, *Nano Lett.*, 11 (2011) 2119.
17. Gurudayal, S. Y. Chiam, M. H. Kumar, P. S. Bassi, H. L. Seng, J. Barber, L. H. Wong, *ACS Appl. Mater. Interfaces*, 6 (2014) 5852.
18. D. Chen, Z. Liu, *ChemSusChem*, 11 (2018) 3438.
19. H. Zhang, D. Li, W. J. Byun, X. Wang, T. J. Shin, H. Y. Jeong, H. Han, C. Li, J.S. Lee, *Nat. Comm.*, 11 (2020) 4622.
20. H. Ahn, K. Yoon, M. Kwak, J. Park, J. Jang, *ACS Catal.*, 8 (2018) 11932.
21. X. Wang, W. Gao, Z. Zhao, L. Zhao, J. P. Claverie, X. Zhang, J. Wang, H. Liu, Y. Sanga, *Appl. Catal. B: Environ.*, 248 (2019) 388.
22. A. Rauf, M. Adil, S. A. Mian, G. Rahman, E. Ahmed, Z. M. Ud Din, W. Qun, *Sci. Rep.*, 11, 41 (2021). <https://doi.org/10.1038/s41598-020-78824-y>
23. A. Subramanian, E. Gracia-Espino, A. Annamalai, H. H. Lee, S. Y. Lee, S. H Choi, J. S. Jang, *Appl. Surf. Sci.*, 427 (2018) 1203.
24. X. Hu, J. Huang, F. Zhao, P. Yi, B. He, Y. Wang, T. Chen, Y. Chen, Z. Li, X. Liu, *J. Mater. Chem. A.*, 8 (2020) 14915.
25. C. Liu, Y. Fu, Y. Xia, C. Zhu, L. Hu, K. Zhang, H. Wu, H. Huang, Y. Liu, T. Xie, J. Zhong, Z. Zang, *Nanoscale*, 10 (2018) 2454.
26. D. Chu, K. Li, A. Liu, J. Huang, C. Zhang, P. Yang, Y. Du, C. Lu, *Int. J. Hydrog. Energy*, 43 (2018) 7307.
27. M. P. Cardona, M. Li, J. McCall, D. Wang, Y. Li, C. Yang, *Mater. Today Energy*, 8 (2018) 8.
28. B. C. Faust, M. R. Hoffmann, D. W. Bahnemann, *J. Phys. Chem.*, 93 (1989) 6371.
29. A. K. S. Kumar, Y. Zhang, D. Li, R. G. Compton, *Electrochem. Commun.*, 121 (2020) 106867.
30. A. P. Araujo, O. S. G. P. Soares, A. J. S. Fernandes, M. F. R. Pereira, C. Freire, *RSC Adv.*, 7 (2017) 14290.
31. A. Rufus, N. Sreeju, D. Philip, *RSC Adv.*, 6 (2016) 94206.
32. K. Jurewicz, C. Vix-Guterl, E. Frackowiak, S. Saadallah, M. Reda, J. Parmentier, J. Patarin, F. Béguin, *J. Phys. Chem. Solids*, 65 (2004) 287.
33. R. Barik, B. K. Jena, A. Dash, M. Mohapatra, *RSC Adv.*, 4 (2014) 18827.
34. B. Xu, S. Yue, Z. Sui, X. Zhang, S. Hou, G. Cao, Y. Yang, *Energy Environ. Sci.*, 4 (2011) 2826.
35. E. Thimsen, F. Le Formal, M. Grätzel, S. C. Warren, *Nano Lett.*, 11 (2011) 35.
36. S. Park, H. J. Kim, C. W. Lee, H. J. Song, S. S. Shin, S. W. Seo, H. K. Park, S. Lee, D. Kim, K. S. Hong, *Inter. J. Hydrog. Energy*, 39 (2014) 16459.
37. R. Zhang, Y. Fang, T. Chen, F. Qu, Z. Liu, G. Du, A. M. Asiri, T. Gao, X. Sun, *ACS Sustainable*

Chem. Eng., 5 (2017) 7502.

38. H. Li, M. Yin, X. Li, R. Mo, *ChemCatChem*, 14 (2021) 2331.

39. L. Yang, C. Yao, R. Wang, L. Jiang, W. Zhu, M. Wang, L. Liu, D. Liang, L. Hu, C. Den, Q. Yin, M. Zhang, G. He, J. Lv, Z. Sun, *Mater. Chem. Phys.*, 275 (2022) 125226.

40. H. Han, J. Chen, L. Wen, J. Liu, *Catal. Lett.*, (2022) 10.1007/s10562-021-03909-w.

© 2022 The Authors. Published by ESG (www.electrochemsci.org). This article is an open access article distributed under the terms and conditions of the Creative Commons Attribution license (<http://creativecommons.org/licenses/by/4.0/>).